8

Motion Estimation of Moving Target using Multiple Images in Intelligent Space

TaeSeok Jin[1] and Hideki Hashimoto[2]
[1]*Dept. of Mechatronics Engineering, DongSeo University,*
[2]*Institute of Industrial Science, the University of Tokyo*
[1]*Korea,* [2]*Japan*

1. Introduction

During the past two decades, researchers in mobile robotics have dealt with different path planning methods. In most cases, the methods goal is to find free collision paths; which will meet the initial and final configurations to complete a mission. Some researchers have proposed methods where the robot's configuration is perfectly known at each instant during the planning and navigation stages(Moreno & Dapena, 2003) . This is not always possible. Dealing with uncertainty, in the planning stage, is essential when the position errors values approach values close to the allowed thresholds for the mission. Plans based on geometrical models, assuming null uncertainty, are clearly insufficient when the mobile robot has to coexist with humans or other kind of difficult situations. Thus, the use of planners, which not explicitly deal with uncertainty, is limited to simple situations, where the errors are less than the allowed thresholds to accomplish the missions (Bouilly & Siméon, 1996). In general, the basic requirements for the autonomous navigation of a mobile robot are environmental recognition, path planning, driving control and location estimation/correction capabilities (Nakamura, 1991, Haralick & Shapiro). The location estimation and correction capabilities are practically indispensable for the autonomous mobile robot to execute the given tasks efficiently. There are many factors involved in obtaining accurate location information while the mobile robot is moving (Sim & Dudek). To get reliable and precise location data, sensor fusion techniques (Ayache & Faugeras, 1989, Zhou & Sakane, 2001) have also been developed. When a CCD camera is utilized under good illumination conditions, certain patterns or shapes of objects are also effective for determining the location (Han et.al, 1999, Segvic & Ribaric, 2001). Similarly when a mobile robot is moving in a building, the walls, edges, and doors can be utilized for position estimation (Betke, 1994 David, 1989). Most researches (Choset, 2001, Sanisa, 2001, Philippe & Colle, 2001) focus on the indoor navigation of a mobile robot in a well-structured environment. In other words, beacons, doors, and corridor edges are utilized to estimate the current location of the mobile robot. However, in cases such as when a mobile robot is navigating under a deep sea or in a forest (Kim, et.al, 2001), there are no landmarks that can be utilized to determine the location.
This paper considers the situations where a mobile robot and a walking human coexist in a structured intelligent environment, such as assembly line in a factory. In these cases, one cannot utilize any landmarks or special features known *a priori* (Lallet & Lacroix, 1998,

Olson, 2000) to localize the mobile robot. The only thing that can be utilized for the localization is the information on a human captured by a CCD camera attached on top of the mobile robot. And an intelligent environment is used in order to solve these problems, a new scheme for the mobile robot localization using the information on the moving object has been developed. This situation might be considered as the inverse of tracking of an unknown moving object using a navigating robot with a camera whose location is precisely calibrated and stored all the time. The tracking problem has been already tackled in many researches (Nair & Aggarwal, 1989).

In this research, the data coming from the dead reckoning sensors are used to obtain the initial location of the mobile robot and it is corrected through the position estimation procedure using the information on the moving object/walking human. For the quantitative analysis of this approach, the position uncertainty of the mobile robot (Adam & Rivlin, 2000, Caglioti, 2001) is represented by an uncertainty ellipsoid that shows the directional uncertainty quantitatively. The trajectory of the moving object is transformed to the image frame and represented as a geometrical constraint equation that is used for the Kalman filtering process (Kalman, 1960, Sorenson, 1966) that estimates the position of the mobile robot to reduce the size of the uncertainty ellipsoid. And a mobile robot cooperates with multiple intelligent sensors, which are distributed in the environment. The distributed sensors recognize the mobile robot and the moving objects/walking human, and give control commands to the mobile robot. The mobile robot receives the necessary support for localization control from the environmental sensors. We aim to perform mobile robot localization without applying any burden to the human with a mobile robot that is simple in structure. We propose intelligent space (ISpace) as an intelligent environment with many intelligent sensors, and are building an environment where humans and mobile robots can now coexist. The mobile robot of this research is one of the physical agents for human support in ISpace (Lee & Hashimoto, 2001).

This paper is organized as follows. In Section 2, the concept of ISpace and the robot localization in intelligent space are explained. Section 3 describes the driving model of a mobile robot and the position estimation uncertainty. In Section 4, the image transformation relation, image projection of the walking human' trajectory, and the position correction technique using the Kalman filter are described. Section 5 explains the proposed control method is applied to ISpace. The simulations and the experiments of robot localization are performed and the effect of the proposed method is verified. Finally, the Conclusions and directions for future work are described in Section 6.

2. Robot Localization in Intelligent Space

2.1 Structure of ISpace

ISpace is a space where many intelligent devices are distributed throughout the whole of the space, as shown in Fig. 1. These intelligent devices have sensing, processing and networking functions, and are named distributed intelligent networked devices (DINDs). These devices observe the positions and behavior of both humans and robots coexisting in the ISpace. The information acquired by each DIND is shared among the DINDs through the network communication system. Based on the accumulated information, the environment as a system is able to understand the intention of humans. For supporting humans, the environment/system utilizes machines including computers and robots.

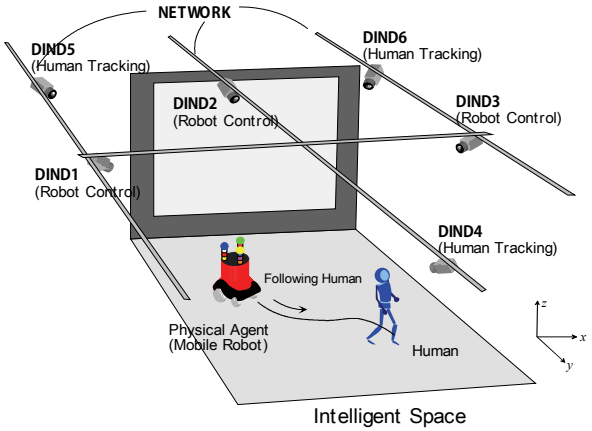

Figure 1. Structure of Intelligent environment by distributed cameras

2.2 ISpace System with Multi-camera

In ISpace, the CCD camera is adopted as the sensor for DINDs, and the tracking of moving objects, such as walking human, and mobile robot, is performed. There are two advantages in using CCD cameras. One is that the position measurement of the targets is a noncontact method. The other is that the human doesn't have to carry any special devices for the DINDs to be able to measure his position. Experiments were performed in the laboratory room, which is about 7 m in both width and depth, is used for the ISpace. The ISpace has a mobile robot as a human-following agent, six DINDs which can obtain the situation in the environment, and a projector and a screen which present suitable information to the human. Each module is connected through the network communication. Three DINDs are used in order to recognize the mobile robot and to generate the control commands. The other three DINDs are used to recognize the position of the human. DINDs are placed as shown in Fig. 1.

In the Intelligent Space, the DIND understands events occurring within the space and offers appropriate services for people by using devices such as robots, displays, and speakers. We can avoid the redundancy of function by sharing the information obtained by the DINDs and assigning each DIND to either recognize a walking human or a robot. The recognition and control performance in 3-D space were improved by locating each DIND for a walking human or robot using the position of triangular form. This intelligence, obtained spatially by the DINDs, connects the physical and digital spaces and enables the understanding of the human's motion.

Fig. 2 is a picture of the actual ISpace. The placement of the three DINDs for human recognition is optimized to expand the viewable area of the cameras so that the head and hands of the human can be recognized over a wide area (Akiyama, Lee, & Hashimoto, 2002). On the other hand, the placement of DINDs for the mobile robot has to be decided by trial and error. It is desirable that the DINDs for the mobile robot recognize the whole of the area covered by three DINDs for human recognition in order to achieve the human-following system and reliable mobile robot control. Thus, three DINDs are placed so that the area for human recognition is completely covered. Human walking information is extracted by

background subtraction and by detecting the skin color of a face and hands on captured images.

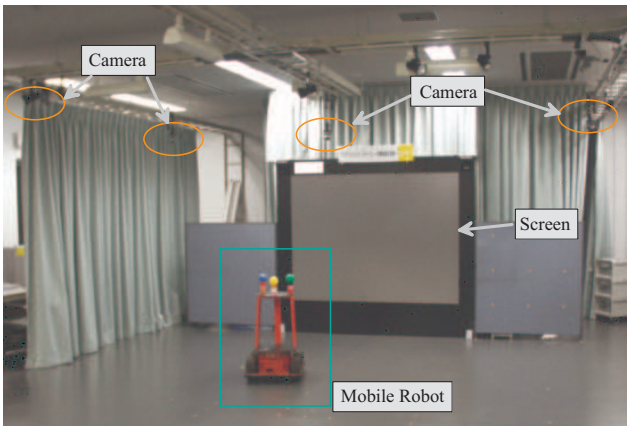

Figure 2. Experimental environment

A mobile robot is connected to the DIND network via wireless LAN, as shown in Fig. 3, and shares the resources of the DIND's. For recognizing the position of the robot, one color panels are installed around the mobile robot. The pattern of the color panel is recognized by the DIND and it estimates the posture and position of the robot by kinematics of robot projected onto an image plane. Since the height of the mobile robot is already known, the position of a mobile robot is reconstructed from one camera image.

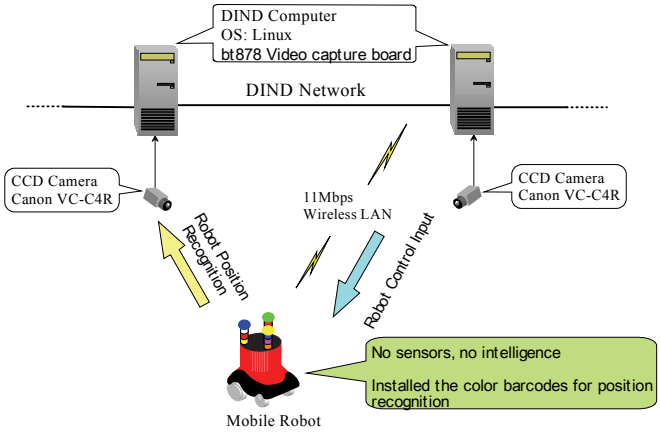

Figure 3. Mobile robot and network system in ISpace

3. Position Uncertainty Modeling

3.1 Ellipsoid point with uncertainty ellipse

The "ellipsoid point with uncertainty ellipse" is characterized by the coordinates of an ellipsoid point (the origin), distances $r1$ and $r2$, and the angle of orientation A. It formally describes the set of points on the ellipsoid that fall within or on the boundary of an ellipse

with semi-major axis of length *r*1 oriented at angle A (0 to 180o) measure d clockwise from the north and semi-minor axis of length *r*2. The distances are the geodesic distances over the ellipsoid, i.e., the minimum length of a path on the ellipsoid that joins the two points, as shown in Fig. 5(4).
The ellipsoid point can be used to indicate points on the Earth's surface or near the Earth's surface that have the same latitude and longitude. The confidence level with which the position of a target entity is included within this set of points is also specified along with this shape. The typical use of this shape is to indicate a point when its position is known only with a limited accuracy, but the geometrical contributions to uncertainty can be quantified.

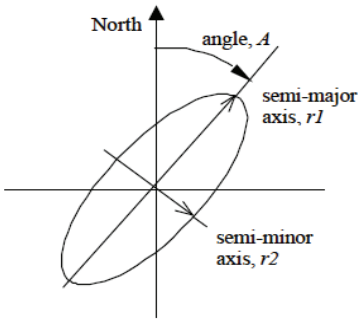

Figure 4. Description of an uncertainty ellipse

Mathematically, an ellipsoid E^t is a region of space defined as follows:

$$E^t := \{\mathbf{x} \in \mathbf{R}^n : (\tilde{\mathbf{x}_o}\mathbf{x}_m) P_t^{-1} (\tilde{\mathbf{x}_o}\mathbf{x}_m) \leq 1.0 \}, \quad (1)$$

for some $\mathbf{x} \in \mathbf{R}^n$, where the subscripts **o** and **m** represent the observed point and the point in the map, respectively. Pt is a symmetric and positive definite matrix.
The aim of the ellipsoid method is to begin with a large ellipsoid (usually an n-dimensional sphere where n is a dimension of a state space) that contains the whole uncertainty set and to then generate a sequence of progressively smaller/larger ellipsoids, leading to an ellipsoid that fits the state uncertainty as tightly as possible.
The positional uncertainty of the object point in world coordinates is calculated by first applying the rotation between the robot and the world coordinates and then adding the uncertainty of the robot position. In order to determine the correspondence between the observation and the map, we integrate the observation result with the map to reduce the positional uncertainty of object points. For this purpose, we need to determine the correspondence between the object points in the observed data and those in the map. For each observed point, we identify the corresponding point on the map that satisfies the Eq. (1).

3.2 Modeling of Mobile Robot

The initial position of a mobile robot can be specified precisely. However, measurement error and slippage during the movement may cause the position estimation uncertainty to be large. This uncertainty increases with driving distance, and may eventually result in losing the location of the mobile robot.

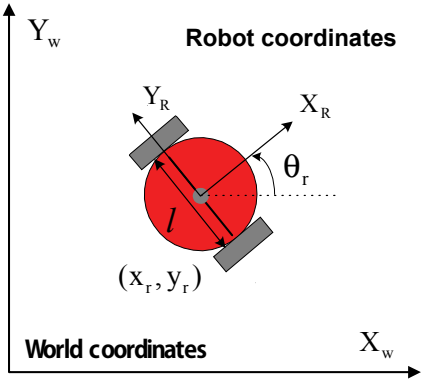

Figure 5. Geometrical model of a mobile robot

The robot's position will be represented by the vector of its spatial variables $\mathbf{x}(k)$, as a point in the Cartesian plane, with $x_r(k)$ and $y_r(k)$ coordinates and an orientation $\theta_r(k)$, $\mathbf{x} = [x_r, y_r, \theta_r]^T$. The simplified kinematic model proposed in (Adam, Rivlin & Shimshoni, 2000) describes how the robot's position changes in time, in relation to an initial position, in response to a $\mathbf{u}(k)$ control input formed by a $T(k)$ translation followed by a $\theta_r(k)$ rotation: $\mathbf{u}(k) = [T(k), \theta_r(k)]^T$. The state, for a given instant, is obtained from the state transition function $f(\mathbf{x}(k), \mathbf{u}(k))$, represented in Eq. (2)

$$\begin{aligned} \mathbf{x}(k+1) &= f(\mathbf{x}(k), \mathbf{u}(k)) + \mathbf{v}(k) \\ &= \begin{bmatrix} x_r(k) + T(k)\cos(\theta_r(k)) \\ y_r(k) + T(k)\sin(\theta_r(k)) \\ \theta_r(k) + \Delta\theta(k) \end{bmatrix} + \mathbf{v}(k) \end{aligned} \tag{2}$$

where $f(\mathbf{x}(k), \mathbf{u}(k))$, is a non-linear state transition function, $\mathbf{v}(k)$ is a noise source assumed to be zero-mean Gaussian with covariance $\mathbf{Q}(k) \rightarrow N(0, Q(k))$ and finally $\mathbf{u}(k)$ is the control input. The position uncertainty of the robot is modeled by means of a Gaussian distribution of probability centered in the vehicle position at a given moment. Eq. (2) allows to obtain the mean vector estimation in the $k + 1$ position. It is now necessary to estimate the covariance matrix in the same position. The first two moments, the mean and the covariance of the distribution function, which follow the spatial position relationship, must be determined. The covariances matrix related to the prediction, in the non-linear spatial relationship case, is obtained from the Taylor series expansion. Therefore, the estimated position of a mobile robot and $\hat{\mathbf{x}}(k|k)$ covariance matrix equation is shown in Eq. (3) and Eq. (4), respectively (Kalman, 1960).

$$\hat{\mathrm{x}}(k+1) = f(\mathrm{x}(k), \mathrm{u}(k)) \tag{3}$$

$$\mathbf{P}(k+1|k) = \nabla\mathbf{f}\,\mathbf{P}(k|k)\nabla\mathbf{f}^T + \mathbf{Q}(k), \tag{4}$$

where $\nabla \mathbf{f}$ is the state transition function Jacobian, obtained as the linearizing result around the estimated state. The state transition function Jacobian is described in Eq. (5)

$$\nabla \mathrm{f} = \begin{bmatrix} 1 & 0 & T(k)\sin(\hat{\theta}_r(k \mid k)) \\ 0 & 1 & T(k)\cos(\hat{\theta}_r(k \mid k)) \\ 0 & 0 & 1 \end{bmatrix}. \tag{5}$$

In order to estimate the vehicle position, odometry is not enough. The $\hat{x}(k \mid k)$ covariance matrix equation shown in Eq. (4) tends to grow continuously (Fig. 6). Using this covariance matrix, the position estimation uncertainty can be represented as a hyper-ellipsoid. That is, the uncertainty hyper-ellipsoid can be defined (Nakamura, 1991) from the SVD (singular value decomposition) of the covariance matrix. This SVD provides the principal axis by the left singular vectors and the length along the axis by the corresponding singular values. Fig. 6 illustrates the effectiveness of the uncertainty ellipsoid as an example. It shows that the uncertainty ellipsoid becomes larger with the movement of a mobile robot, and that the geometrical shape of the ellipsoid directly represents the position estimation uncertainty along a given axis.

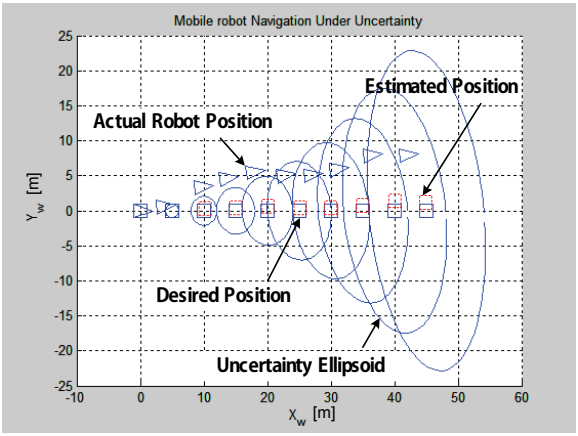

Figure 6. Uncertainty ellipsoids with the movement of a mobile robot

4. Position Estimation based DINDs

4.1 Image projection of walking human

During navigation, a mobile robot may need to re-locate its position. When there is a walking human that can be captured by the CCD camera of DINDs and the motion information on the walking human is available to the mobile robot, it may stop at its current position to improve the position estimation accuracy of itself by observing the walking human. The given object trajectory can be represented as a linear equation in the image frame, and using the current position estimation of the mobile robot, geometric constraint equations can be derived through coordinate transformation.

The derivation procedure of geometric constraint equations is going to be illustrated with an example shown in Fig. 7. The conventional pin-hole model (Haralick & Shapiro, 1993) is utilized to form a geometrical model of the camera. In Fig. 7, $(x_W \;\; y_W \;\; z_W)$ and (u, v) represent the reference coordinates and the image coordinates, respectively.

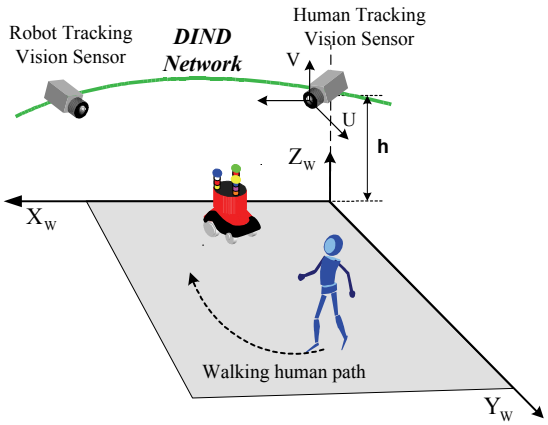

Figure 7. Coordinates for a walking object and a mobile robot

The walking human is assumed to have the following trajectory on the $x_W - y_W$ plane of the reference coordinates, without loss of generality:

$$f(x_W, y_W) = 0 \tag{6}$$

where $z_W (= z_0 \neq h)$ is also assumed to be constant and not equal to the camera height, h.

The walking human trajectory in the reference coordinates can then be transformed into the robot coordinates, as follows:

$$\begin{bmatrix} x_R \\ y_R \\ z_R \end{bmatrix} = \begin{bmatrix} \cos\hat{\theta}_r & \sin\hat{\theta}_r & 0 \\ -\sin\hat{\theta}_r & \cos\hat{\theta}_r & 0 \\ 0 & 0 & 1 \end{bmatrix} \begin{bmatrix} x_W - \hat{x}_r \\ y_W - \hat{y}_r \\ z_W \end{bmatrix} \tag{7}$$

where $[\hat{x}_r \;\; \hat{y}_r \;\; \hat{z}_r]^T$ represents the current estimated position of the mobile robot and $[x_W \;\; y_W \;\; z_W]^T$ represents the position of the walking human.

This point ($[x_R \;\; y_R \;\; z_R]^T$) is again mapped onto the image frame using the perspective projection, as follows (Haralick & Shapiro, 1993, Han et.al, 1999):

$$\begin{bmatrix} u \\ v \end{bmatrix} = \begin{bmatrix} \lambda \dfrac{y_R}{x_R} \\ \lambda \dfrac{z_R - h}{x_R} \end{bmatrix} \tag{8}$$

where λ represents the camera focal length, and $z = [u \quad v]^T$ is the position of the walking human on the image frame. Based on the equations (7) and (8), the geometric constraint equation can be generally represented as

$$f(z, \hat{x}) = 0 \tag{9}$$

where $\hat{x} = [x_r, y_r, \hat{z}_r]^T$ represents the current estimated position of the mobile robot.

4.2 Position Correction

The calculated position of the walking human in the image frame, based on the estimated robot position, has some discrepancy from the actual value. Utilizing this error, the practical position of the robot can be corrected recursively. To overcome vague input information, *i.e.*, the human position in the image frame includes noise and the position estimation of the robot has uncertain components, the Kalman filtering technique is adopted to form a robust observer (Kalman, 1960, Sorenson, 1966). The geometric constraint equations between the human image coordinates and the robot position are approximated to a linear system equation, and the Kalman filtering technique is applied to estimate the robot position.

It is assumed that i-th measured vector, *i.e.*, the position of the walking human, $\hat{z}_i$, includes noise with the following average and variance:

$$\hat{z}_i = z_i + \nu_i \tag{10}$$

where $E[\nu_i] = 0$ and $E[\nu_i \nu_i^T] = S_i$.

The nonlinear constraint equations are approximated to linear ones using the Taylor series expansion, ignoring the higher order nonlinear terms at the measured vector, $\hat{z}_i$, and the estimated position of the mobile robot, $\hat{x}_{i-1}$. That is,

$$\begin{aligned} & f(z_i, \hat{x}) = 0 \\ & \approx f(\hat{z}_i, \hat{x}_{i-1}) + \left.\frac{\partial f}{\partial z}\right|_{z=\hat{z}_i} (z_i - \hat{z}_i) + \left.\frac{\partial f}{\partial \hat{x}}\right|_{\hat{x}=\hat{x}_{x-1}} (\hat{x} - \hat{x}_{i-1}) \end{aligned} \tag{11}$$

where $\left.\dfrac{\partial f}{\partial z}\right|_{z=\hat{z}_i}$ and $\left.\dfrac{\partial f}{\partial \hat{x}}\right|_{\hat{x}=\hat{x}_{i-1}}$ represent the estimated value of $\dfrac{\partial f}{\partial z}$ and $\dfrac{\partial f}{\partial \hat{x}}$ at $\hat{z}_i$ and $\hat{x}_{i-1}$, respectively.

For a linear system, the equation (11) can be rearranged as the following matrix equation (Ayache & Faugeras, 1989).

$$y_i = M_i \hat{x} + u_i \tag{12}$$

where $y_i = -f(\hat{z}_i, \hat{x}_{i-1}) + \left.\frac{\partial f}{\partial \hat{x}}\right|_{\hat{x}=\hat{x}_{i-1}} \hat{x}_{i-1}$, $M_i = \left.\frac{\partial f}{\partial \hat{x}}\right|_{\hat{x}=\hat{x}_{i-1}}$ and $u_i = \left.\frac{\partial f}{\partial z}\right|_{z=\hat{z}_i} (z_i - \hat{z}_i)$.

In this equation, y_i becomes the new measured vector, M_i combines the measured vector and the robot position, $\hat{x}$, linearly, and u_i is the error for linearization of the measured vector with the following average and variance values (Nakamura, 1991).

$$E[u_i] = 0 \tag{13}$$

$$E[u_i u_i^T] = W_i = \frac{\partial \hat{f}}{\partial z} S_i \frac{\partial \hat{f}}{\partial z}^T \tag{14}$$

Since M_i and y_i are *a priori* given values, if we have the average and variance of u_i, we can obtain the optimal estimated value of $\hat{x}$ with the new variance. The Kalman filter provides the estimated value, $\hat{x}$, which minimizes the expected squared error norm, $E[(\hat{x}-x)^T(\hat{x}-x)]$ as the linear combination of the measured vectors, $\{y_i\}$, as follows:

$$\hat{x}_i = \hat{x}_{i-1} + K_i(y_i - M_i \hat{x}_{i-1}) \tag{15}$$

$$K_i = P_{i-1} M_i^T (M_i P_{i-1} M_i^T + W_i)^{-1} \tag{16}$$

$$P_i = (I - K_i M_i) P_{i-1} \tag{17}$$

where K_i represents the Kalman gain, P_i is the zero-mean-variance matrix of the estimated error by the ith measured vector, and $\hat{x}_i$ is the estimated robot position by the ith measured vector.

The initial robot position estimation and variance, $\hat{x}_0$ and P_0, can be obtained using the mobile robot driving model. Using the *n* image frames from the image coordinates of the moving object, the final robot position is recursively estimated as $\hat{x}_n$, with a variance of P_n.

5. Simulation and Experiments

5.1 Simulation

The simulations were performed for two different patterns of walking human motion: the parabolic motion and the sinusoidal motion. To make it realistic, the following camera parameters in Table 1 were utilized:

Parameter	value
Camera height (h)	$220\,cm$
Focal length (λ)	$1.25\,cm$
CCD size $(H)\times(V)$	$0.66\,cm\times 0.48\,cm$

Table 1. The parameters of camera system

The variances of the measured vectors were independent of each other; the empirical variances were obtained as follows:

$$S_i = \begin{bmatrix} 0.005^2 & 0 \\ 0 & 0.005^2 \end{bmatrix}. \tag{18}$$

The estimated initial position and the error variance came from a mobile robot driving model with 100 msec of control cycle, where the input errors of the wheel angle readings are limited to within 2% for Kalman filtering.

Case 1: a parabolic walking motion case

As the simplest example, an object was assumed to be moving along a parabolic curve, specified as the range, $X_w = 400 - 600[cm]$, $Y_w = -0.1(X_w - 500)^2 + 1200[cm]$, $Z_w = 100[cm]$, walking speed: 30 Cm/sec.

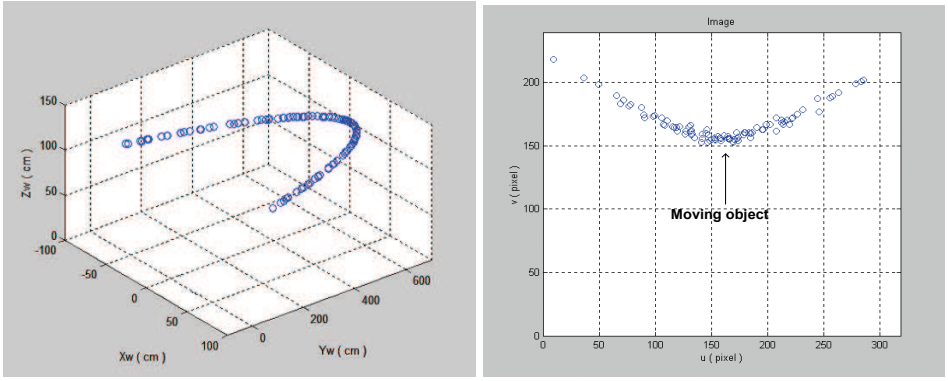

(a) Trajectory of moving object (b) Image coordinates of a moving object

Figure 8. Moving object trace on the image frame

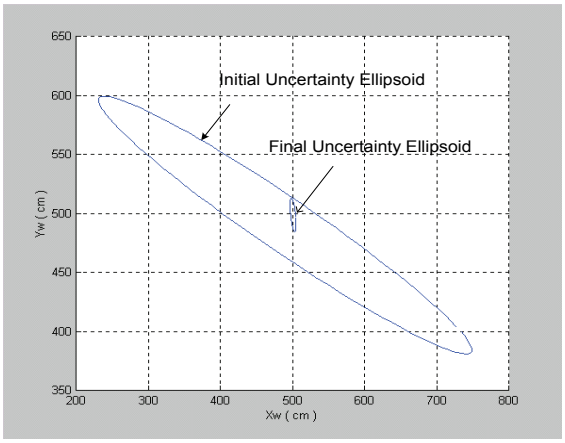

Figure 9. Improvement of position estimation uncertainty

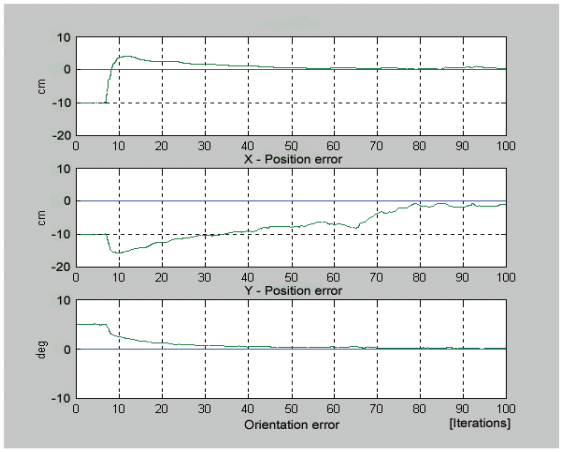

Figure 10. Position estimation errors

Fig. 8 (a)-(b) represents the moving path of the walking human in 3-D space and on the image frame respectively, and Fig. 9 shows the quantitative improvement of the position estimation uncertainty. Finally, Fig. 10 represents the position estimation error for each component of the robot position, (x,y,θ) when the parabolic walking motion is utilized for the localization. Note that since the walking human provides the useful information useful for the position correction on the x-y plane, the uncertainty ellipsoid shrunk along all directions, as shown in Fig. 9. Also notice that both of the x and y position errors of the robot converse to zero for the same reason, as shown in Fig. 10. The position estimations and zero-mean variances before and after the 100 times iterations are shown as:

Initial: $\hat{x}_0 = [490cm \quad 480.5cm \quad 95°]^T$ and $P_0 = \begin{bmatrix} 243.1162 & -89.8719 & -0.6576 \\ -89.8719 & 62.9118 & 0.2529 \\ -0.6576 & 0.2529 & 0.0105 \end{bmatrix}$

Final: $\hat{x}_{100} = [500.4cm \quad 499.6cm \quad 90.2°]^T$ and $P_{100} = \begin{bmatrix} 3.6294 & -2.1574 & 0.0080 \\ -2.1574 & 15.4273 & -0.0044 \\ 0.0080 & -0.0044 & 0 \end{bmatrix}$.

Note that the estimated position, $\hat{x}_{100} = [500.4cm \quad 499.6cm \quad 90.2°]^T$, converges to the real position, $x = [500cm \; 500cm \; 90°]^T$ precisely.

Case 2: a sinusoidal walking motion case

As a general case, the trajectory of a walking human was assumed to be a sinusoidal trajectory, represented as follows:

$X_w = 400 - 600[cm]$, $Y_w = -0.01(X_w - 500)^3 + 300[cm]$, $Z_w = 100[cm]$, walking speed: 30 Cm/sec.

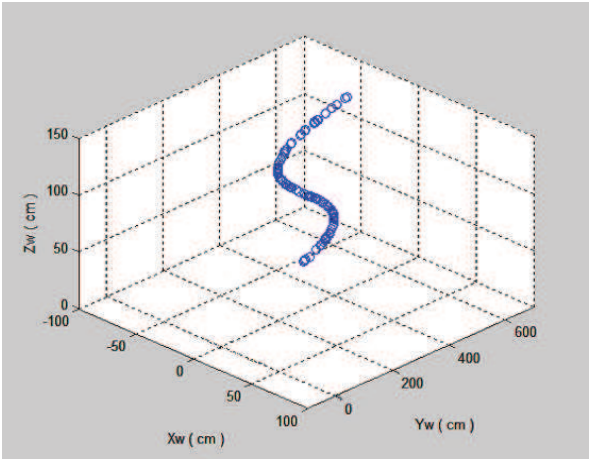

(a) Trajectory of moving object

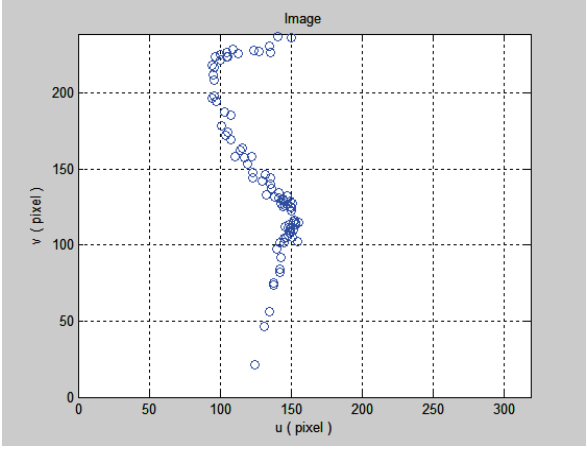

(b) Image coordinates of a moving object

Figure 11. Moving object trace on the image frame

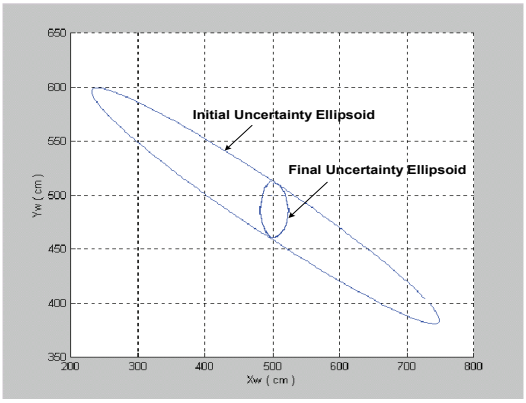

Figure 12. Improvement of position estimation uncertainty

Fig. 11 (a)-(b) represents the sinusoidal moving path of the walking human and the image coordinates of a moving object respectively, and Fig. 12 shows the uncertainty ellipsoid for moving object closer to the walking human tends to be smaller, as expected for visual information with updated estimation. Finally, Fig. 13 represents the position error and the orientation error for each component of the robot position respectively. These simulation results indicate that the Multi-visual estimation correspond well to actual objects in the ISpace.

Initial: $\hat{x}_0 = [490cm \quad 480cm \quad 95°]^T$ and $P_0 = \begin{bmatrix} 242.9162 & -89.7719 & -0.5576 \\ -89.7719 & 62.3118 & 0.1829 \\ -0.5576 & 0.1829 & 0.0015 \end{bmatrix}$

Final: $\hat{x}_{100} = [503.4cm \quad 504.0cm \quad 90.2°]^T$ and $P_{100} = \begin{bmatrix} 5.7384 & -2.2684 & 0.0180 \\ -2.2684 & 15.8873 & -0.0174 \\ 0.0180 & -0.0174 & 0 \end{bmatrix}$.

Note that the estimated position, $\hat{x}_{100} = [503.4cm \quad 504.0cm \quad 90.2°]^T$, converges to the real position, $x = [500cm \; 500cm \; 90°]^T$ precisely.

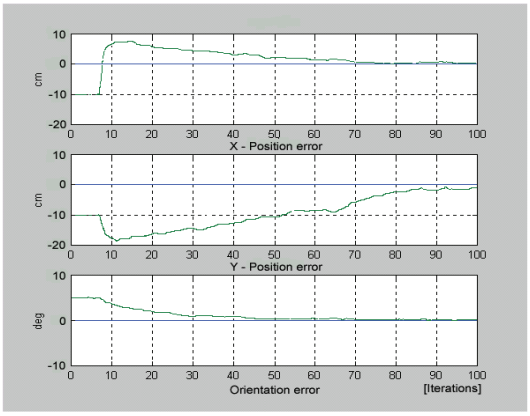

Figure 13. Position estimation errors

5.2 Experiments

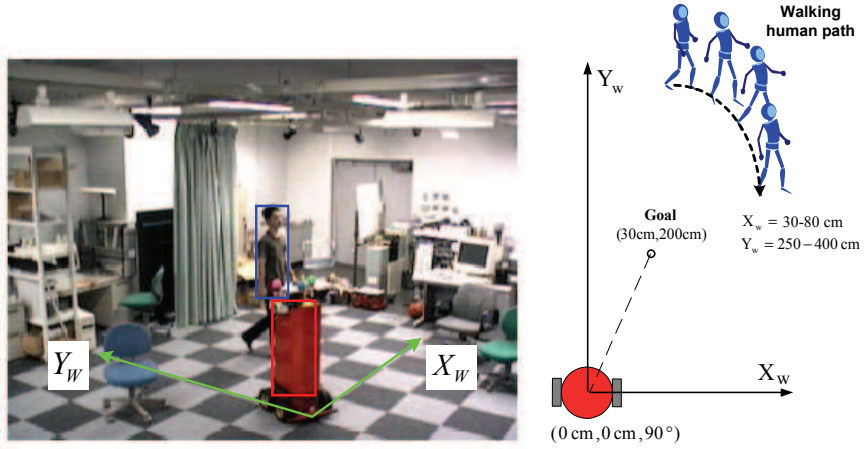

Figure 14. Experimental environment

The real experiments were performed at the ISpace as shown in Fig. 2. In this experiment, the robot is driven to follow walking human in the ISpace. The initial position of the mobile robot was set as (0 cm, 0 cm, 90°) and aimed towards the goal position, (30 cm, 200 cm, 90°), where the CCD camera of DIND tracks the walking human on the floor to correct its own position. The trajectory of the walking human was captured by a color CCD camera, VC-C4R, made by CANON Inc. and the trace was given as $X_w = 30-80[cm]$, $Y_w = 250-400[cm]$, and $Z_w = 100[cm]$ with the speed of 100 Cm/sec. The parameters used for the experiments were the same as for the simulations. When the robot arrived at the goal position, it captured 20 frames of images every 100 msec for the walking human to estimate and correct its own position utilizing the information on the walking human. The real position of the mobile robot was $[33cm \quad 208cm \quad 90°]^T$, and the estimated position of the mobile robot and the variance of the estimated error were given as

$$\hat{x}_0 = [28cm \quad 195cm \quad 87.9°]^T \text{ and } P_0 = \begin{bmatrix} 49.951 & -1.021 & -0.154 \\ -1.021 & 0.183 & 0.003 \\ -0.154 & 0.003 & 0.001 \end{bmatrix}.$$

After the 100 frames of observation, the estimated position of the mobile robot became very close to the real position, and the variance of the estimated error was greatly reduced, as shown below:

$$\hat{x}_{100} = [29.4cm \quad 196.4cm \quad 89.7°]^T \text{ and } P_{100} = \begin{bmatrix} 8.0406 & -0.1784 & 0.0252 \\ -0.1784 & 0.1660 & -0.0006 \\ 0.0252 & -0.0006 & 0.0001 \end{bmatrix}.$$

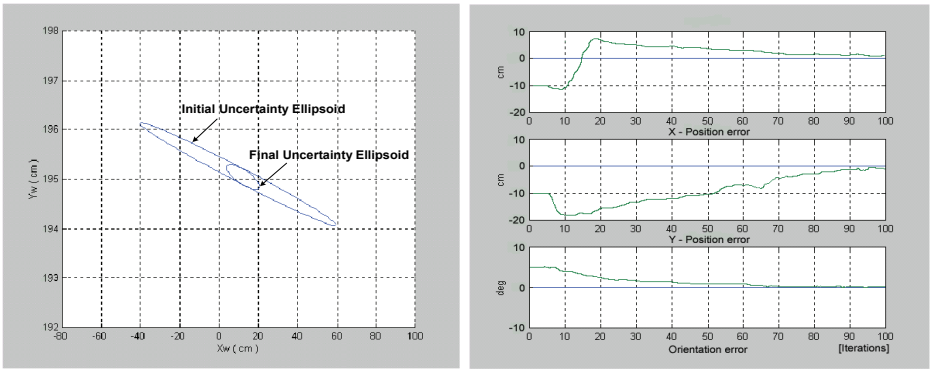

(a) Robot position estimation uncertainty (b) Position errors

Figure 15. Improvement of position estimation uncertainty

The robot position estimation uncertainty was represented as an uncertainty ellipsoid and it was very impressive that the size of the ellipsoid shrunk only along the normal direction of the walking human, as shown in Fig. 15 (a). Fig 15(b) shows the position errors of the mobile robot. As expected, we can see that the position error reduced significantly as the robot moves, depending on the motion it observes. The overall robot pose uncertainty for each cycle decreases over iterations, showing that by observing the scene repeatedly with DINDs, the estimation uncertainty reduces and hence a better robot pose is obtained. The robot orientation also decreases slightly for this reason, when walking motion has not acute angle turn.

These experimental results correspond to the experiment performed inside the 7 m x 7 m space. Evidently, in the experiment, the simulation error range appears low since the mobile robot and the walking human were assumed to be point objects, and the size of point was set to 30 cm x 100 cm. Moreover, the simulation result is better than the experimental result because of the following factors in the real experiment: nonlinear elements in the motion of walking human, the robot position error due to wheel slippage, rough surface, and sensor error.

As regards the additional experimental results, Fig. 16 presents the experimental results with respect to walking speed for case 1. For comparison purposes, the Kalman filter was also designed based on case 1, and its outputs are plotted in the figure. The walking human moved along a parabolic trajectory in the x-y axis, and the motion models had the same zero-mean variance. Fig. 16(a) shows the data plot of the localization error when only the constraints imposed by the visibility regions are used. As evident from the figure, the DIND system is unable to localize the mobile robot based on this information alone. Moreover, when the average walking speed is 100 cm/s, the localization accuracy is reasonably high and the robot is capable of quickly determining its absolute position in the environment.

Fig. 16(b) presents the experimental result when the walking speed is above 110 cm/s and the turns of human are included. When the walking human accelerates, the DIND4, DIND5, and DIND6 are used to track the accurate position and direction of the human. As compared to Fig. 16, the response of the position is reasonably smooth, whereas the orientation continues to be very noisy during the sampling step 30. This is due to distortions of the

images caused by the human's motion and walking speed. During the sampling step of 90 ms, the position error is at most 100 mm, and the orientation error is up to 5 degrees.
In future research efforts, it is necessary to examine the influence of the mobile robot, which maintains a flexible distance between the robot and the human. In the ISpace, since a human-walking trajectory is newly generated at every step, it is considered to be a function of time. Therefore, the application of tracking control is effective. However, although the target trajectory of a mobile robot is continuous and smooth when the usual tracking control is applied, the actual human-walking trajectory that is to be tracked by the robot is generally unstable. In such cases, stable human-following behavior may not be achieved by the usual tracking control.

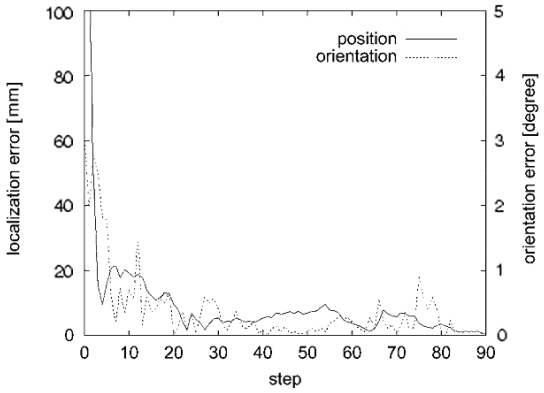

(a) Position and orientation error at an average speed of 100 cm/s

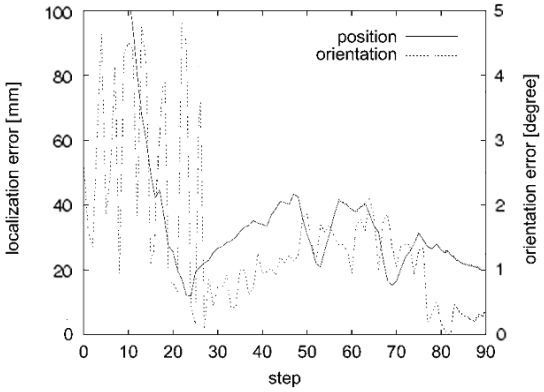

(b) Position and orientation error at an average speed of above 110 cm/s

Figure 16. Experimental results of relative human motion

6. Conclusion

In this paper, using the images of walking human, an absolute position estimation method for a human following robot in ISpace was presented. First, the position estimation uncertainty of the mobile robot is quantitatively represented by the uncertainty ellipsoid.

The real human position is transformed to geometric constraint equations in the image coordinates for a given robot position. The control algorithm using the linear constraint equations and the Kalman filtering technique was proposed for a mobile robot in order to estimate and correct its position recursively, and follow a walking human whose position is estimated incompletely.

Specifically, the pre-determined path of a walking human is projected onto an image frame and the geometrical constraint equations between the human's image coordinates and the estimated human following robot position are derived. Since the location is based on the estimated position of the mobile robot, there exists positional discrepancy between the estimated image coordinates and the real position of the walking human. Using this discrepancy, the position of the mobile robot is corrected recursively. Since the image coordinates of the human are subjected to noise, the Kalman filtering technique is adopted for robust estimation. Next, cooperation between the multiple DINDs was described. The position of the human and the mobile robot in ISpace was measured with DINDs. To control a mobile robot in a wide area, cooperation of the DINDs, effective communication and role assignment are required. Finally, simulations and an experiment into the human-following control of a mobile robot were performed using the proposed control algorithm. It was recognized that position estimation accuracy depends on the path of the walking human. The effectiveness of this algorithm is verified through real experiments.

Future studies will involve improving the estimation accuracy for the human following robot and applying this system to complex environments where many people, mobile robots and obstacles coexist. Real time image processing and camera calibration are needed to improve the estimation accuracy for the distance between the human and the mobile robot. Since the proposed algorithm absorbs the kinematic differences between humans and robots, any kind of mobile robot, including legged robots, can be used as human-following robots, as long as the robot is able to move at the speed of human walking. Moreover, it is necessary to survey the influence of the mobile robot which maintains a flexible distance between the robot and the human, and introduces the knowledge of cognitive science and social science.

7. Acknowledgments

This work was supported by the Korea Research Foundation Grant funded by the Korean Government(MOEHRD) (KRF-2007-331-D00152)

8. References

L. Moreno and E. Dapena. (2003). Path quality measure for sensor-based motion planning, *Robotics and Autonomous Systems*, vol. 44, pp. 131-150.

B. Bouilly and T. Siméon. (1996). A sensor-based motion planner for mobile robot navigation with uncertainty, in *Proc. of the International Workshop* on RUR'95, Springer, Berlin, pp. 235–247.

M. Betke *et al*. (1994). Mobile Robot Localization Using Landmarks, *Proc. of the IEEE/ RSJ/GI Int. Conf. on Intelligent Robots and Systems*, pp. 135~142.

J. David, Kreigman *et al*. (1989). Stereo vision and navigation in buildings for mobile robots, *IEEE Trans. Robotics and Automation*, vol. 5, no. 6, pp. 792~803.

J.-H. Lee, G. Appenzeller, and H. Hashimoto. (1997). An agent for intelligent spaces: Functions and roles of mobile robots in sensored, networked, thinking spaces, in *Proc. IEEE Conf. Intelligent Transportation Systems*, Boston, pp. 983–988.

Y. Nakamura. (1991). *Advanced Robotics: Redundancy and Optimization*, Addison-Wesley.

R. M. Haralick and Linda G. Shapiro. (1993). *Computer and Robot Vision*, Addison-Wesley.

N. Ayache and O. D. Faugeras. (1989). Maintaining Representations of the Environment of a Mobile Robot, *IEEE Trans. Robotics and Automation*, vol. 5, no. 6.

R. E. Kalman. (1960). New Approach to Linear Filtering and Prediction Problems, *Trans, ASME, J. Basic Eng*, Series 82D, pp. 35-45.

H. W. Sorenson. (1966). Kalman Filtering Techniques, *Advances in Control Systems Theory and Applications*, vol. 3, pp. 219-292.

M. Y. Han, B. K. Kim, K. H. Kim, and Jang M. Lee. (1999). Active Calibration of the Robot/Camera Pose Using the Circular Objects, in Korean, *Transactions on Control, Automation and Systems Engineering*, vol. 5, no. 3, pp. 314-323.

T. Akiyama, J.-H. Lee, and H. Hashimoto. (2002). Evaluation of CCD camera arrangement for positioning system in intelligent space, in *Proc. Seventh Int. Symp. Artificial Life and Robotics (AROB'02)*, pp. 310–315.

Dinesh Nair and Jagdishkumar K. Aggarwal. (1989). Moving Obstacle Detection From a Navigation Robot, *IEEE Trans. Robotics and Automation*, vol. 14, no. 3, pp. 404~416.

Anthony Lallet and Simon Lacroix. (1998). Toward Real-Time 2D Localization in Outdoor Environments, *Proc. of the 1998 IEEE International Conference on Robotics & Automation*, pp. 2827-2832.

Amit Adam, Ehud Rivlin, and Ilan Shimshoni. (2000). Computing the Sensory Uncertainty Field of a Vision-based Localization Sensor, *Proc. of the 2000 IEEE International Conference on Robotics & Automation*, pp. 2993-2999.

Robert Sim and Gregory Dudek. (1999). Learning Visual Landmarks for Pose Estimation, *Proc. of the 1999 IEEE International Conference on Robotics & Automation,* pp.1972-1978.

B.H. Kim, D.K. Roh, Jang M. Lee, M.H. Lee, K. Son, M.C. Lee, J.W. Choi, and S.H. Han. (2001). Localization of a Mobile Robot using Images of a Moving Target, *Proc. of the 2001 IEEE International Conference on Robotics & Automation*.

Vincenzo Caglioti. (2001). An Entropic Criterion for Minimum Uncertainty Sensing in Recognition and Localization Part II-A Case Study on Directional Distance Measurements, *IEEE Trans. On Systems, Man, and Cybernetics*, vol. 31, no. 2, pp. 197-214.

Clark F. Olson. (2000). Probabilistic Self-Localization for Mobile Robots, *IEEE Trans. On Robotics and Automation*, vol. 16, no. 1, pp.55-66.

Hongjun Zhou and Shigeyuki Sakane. (2001). Sensor Planning for Mobile Robot Localization Based on Probabilistic Inference Using Bayesian Network," *Proc. of the 4th IEEE International Symposium on Assembly and Task Planning*, pp. 7-12.

Muriel Selsis, Christophe Vieren, and Francois Cabestaing. (1995). Automatic Tracking and 3D Localization of Moving Objects by Active Contour Models, *Proc. of the 95' IEEE International Symposium on Intelligent Vehicles,* pp. 96-100.

Howie Choset and Keiji Nagatani. (2001). Topological Simultaneous Localization and Mapping (SLAM): Toward Exact Localization Without Explicit Localization, *IEEE Trans. On Robotics and Automation*, vol. 17, no. 2.

Sanisa Segvic and Slobodan Ribaric. (2001). Determining the Absolute Orientation in a Corridor Using Projective Geometry and Active Vision, *IEEE Trans. On Industrial Electronics*, vol. 48, no. 3, pp. 696-710.

Philippe Hoppernot and Etienne Colle. (2001). Localization and Control of a Rehabilitation Mobile Robot by Close Human-Machine Cooperation, *IEEE Trans. On Neural Systems and Rehabilitation Engineering*, vol. 9, no. 2, pp. 181-190.

J.-H. Lee and H. Hashimoto. (2002). Intelligent space -concept and contents, *Adv. Robot.*, vol. 16, no. 3, pp. 265–280.

Motion Planning

Edited by Xing-Jian Jing

ISBN 978-953-7619-01-5
Hard cover, 598 pages
Publisher InTech
Published online 01, June, 2008
Published in print edition June, 2008

In this book, new results or developments from different research backgrounds and application fields are put together to provide a wide and useful viewpoint on these headed research problems mentioned above, focused on the motion planning problem of mobile ro-bots. These results cover a large range of the problems that are frequently encountered in the motion planning of mobile robots both in theoretical methods and practical applications including obstacle avoidance methods, navigation and localization techniques, environmental modelling or map building methods, and vision signal processing etc. Different methods such as potential fields, reactive behaviours, neural-fuzzy based methods, motion control methods and so on are studied. Through this book and its references, the reader will definitely be able to get a thorough overview on the current research results for this specific topic in robotics. The book is intended for the readers who are interested and active in the field of robotics and especially for those who want to study and develop their own methods in motion/path planning or control for an intelligent robotic system.

How to reference

In order to correctly reference this scholarly work, feel free to copy and paste the following:

TaeSeok Jin and Hideki Hashimoto (2008). Motion Estimation of Moving Target Using Multiple Images in Intelligent Space, Motion Planning, Xing-Jian Jing (Ed.), ISBN: 978-953-7619-01-5, InTech, Available from: http://www.intechopen.com/books/motion_planning/motion_estimation_of_moving_target_using_multiple_images_in_intelligent_space

INTECH
open science | open minds

InTech Europe
University Campus STeP Ri
Slavka Krautzeka 83/A
51000 Rijeka, Croatia
Phone: +385 (51) 770 447
Fax: +385 (51) 686 166
www.intechopen.com

InTech China
Unit 405, Office Block, Hotel Equatorial Shanghai
No.65, Yan An Road (West), Shanghai, 200040, China
中国上海市延安西路65号上海国际贵都大饭店办公楼405单元
Phone: +86-21-62489820
Fax: +86-21-62489821